Report on aspects of variability in high-resolution versions of HadAM3.

Hadley Centre technical note 53

Rachal A. Stratton

23 September 2004

Met Office

Report on aspects of variability in high-resolution versions of HadAM3.

Rachel A. Stratton

Abstract

Variability in HadAM3 is studied by looking at storm tracks. The 17-year AMIP II integrations are used as these consist of a set of runs where both horizontal and vertical resolutions are increased. A variety of methods are used to investigate the mean climatology of storms and processes affecting their development and decay. Results suggest that higher resolution is necessary to provide a better simulation of storms.

1. Introduction

The strength and frequency of storms and how they will change in the future is of great interest to many people. For this reason it is important to ensure that our ability to model the current storm activity is as good as possible. The Hadley Centre's climate model HadAM3 with its relatively low resolution (N48, 2.5° latitude by 3.75° longitude) when compared with current NWP operational forecast models (typically < 1°) does a reasonable job of modelling the large scale characteristics of the storm track regions. The aim of this study is to determine in more detail how well HadAM3 models storms and to investigate whether increasing either horizontal or vertical resolution or both will lead to better simulations.

Typically mid-latitude storms are of order 1000km across whereas our current standard climate model has a resolution ~ 300km at mid-latitudes i.e. the model will attempt to model a storm using a grid of at most 4x4 points. This study looks a doubling and even tripling the horizontal resolution so that a typical storm may be modelled using ~8-12x8-12 points. In the vertical with 19 model levels the tropospheric resolution is currently ~ 100mb; this study looks at increasing this to ~50mb. Work by Pope et al (2000) looking at increasing vertical resolution from 19 to 30 levels considered the need for horizontal and vertical scales to be consistent for accurate representation of atmospheric waves as suggested by (Lindzen and Fox-Rabinovitz 1989). Pope et al (2000) decided that such arguments did not take account of other physical processes, for which a different ranges of vertical and horizontal resolutions to be can be used together.

Information on HadAM3 and the model integrations is provided in section 2. The methods used to investigate storm tracks are outlined in section 3 with the results in section 4.

2. Description of model integrations.

The model used for all the simulations is the Hadley Centre model, HadAM3 described in detail in Pope et al (2000). The standard HadAM3 resolution is N48 with 19 levels. Table 1 below gives the range of other resolution simulations studied. Details of increasing vertical resolution from 19 to 30 levels are given in Pope et al (2001). For full information on the set-up of the increased horizontal resolution runs and a comparison of their mean climate see Pope and Stratton (2002). All the simulations are so called AMIP2 (Atmospheric Model Intercomparison Project number 2) i.e. they run forced with observed sea surface temperatures and sea ice for the period 1979 to 1996 (Gates et al. 1999).

Table of AMIP II integrations available for study

Horizontal Vertical	N48 2.5° x 3.75°	N72 1.67° x 2.5°	N96 1.25° x 1.875°	N144 0.833° x 1.25°
L19	X,S		X	
L30	X,S	X	X,S	X

Key
X – integration available, blank no run at this combination of horizontal and vertical resolution.
S – initial spinup tendencies available

Most of the results shown in this paper are from the N48 and N96 integrations. In section 4.1 the initial spinup tendency runs are used to help understand some of the changes. The initial spinup tendencies were derived by running the model at the resolutions in table 1 from operational analyses from the winter period December 1998 to February 1999. The initial increments of U, V, T and q from the first and second days were meaned and compared. If the difference in the so called "spinup tendencies" looks similar to the difference in the long term means then they can be used to work out which part of the physics or dynamics is causing the change. If the total initial tendencies resemble the model bias then they can be used to help determine which schemes may be contributing to the model error.

3. Methods used to analyse storms

3.1 Verification data.

The AMIP 2 simulations cover a period from 1979-1996. Most of this study makes use of the ERA15 (ECMWF) reanalyses (Gibson et al 1997) covering a 15 year period from 1979 to 1993. In some comparisons the ERA15 analyses have been extend to cover the full 17 years by including ECMWF operational analyses for 1994-1996. ERA15 provides a consistent set of 6 hourly analysis of the main model variables using all available observations. The reliability of the ERA15 analyses depends on the number and quality of the observations. This is much better in northern mid-latitudes than in the Southern Hemisphere so this study tends to concentrate at looking at the Northern Hemisphere storm tracks. In the case of a few mean diagnostics NCEP analyses (Kalnay et al 1996) have also been used for comparison

3.2 Eady parameter.

Storm activity is related to baroclinic instability. Previous studies of storm tracks and cyclone activity (Lindzen and Farrell, 1980, Hoskins & Valdes 1990) have shown that the baroclinicity of the atmosphere can be measured using the maximum Eady growth rate (Eady 1949) defined as

$$\sigma_{BI} = 0.31\left(f / N \right)\left|\partial v / \partial z\right|$$

where f is the Coriolis parameter, N is the static stability, z the vertical coordinate and **v** the horizontal wind vector. In this study the Eady parameter has been calculated using monthly mean data from both the model integrations and ERA and NCEP monthly mean reanalyses.

3.3 Band pass filter

Band pass filters can be used to look at fields on the timescale of synoptic scale features i.e. 2-6 days. The band pass filter used in this study is that described by Doblas-Reyes and Deque (1998) and is applied to a variety of 6 hourly fields output on pressure levels at 850, 700, 500 and 200hPa. The filter picks out scale from 2.5 to 6 days. The band pass data has also been used to evaluate E-vectors (Hoskins et al 1983) at 200 hPa i.e.

$$E = (\overline{v'^2 - u'^2}, -\overline{u'v'})$$

The E-vectors can used used to look at the momentum transport of the storms.

3.4 Feature based analysis of storms.

An alternative method of looking at storms to using a band pass filter is to use a method of feature based tracking. Cyclone development and decay have been analysed using programs provided by Kevin Hodges of Reading University. Details of the methods used in these feature-tracking programs are given in Hoskins and Hodges (2002). For this study we chose to use 6 hourly mean sea level pressure data for the feature tracking. We compared our results with a study of ERA storm tracks done by David Anderson (Anderson et al 2002) also using the same method.

The feature tracking programs work by identifying low pressure centres and tracking them from one 6 hour period to the next. The tracks are recorded over each season and then processed further to derive information on the mean speed of cyclones, where they start, i.e. their genesis, and where they decay, i.e. lysis.

4. Results

4.1 Mean fields

Before looking at the variability at mid-latitudes it is first worth looking at the mean simulation. Detailed information on the changes to the mean fields on increasing horizontal resolution and vertical resolution are available in Pope and Stratton (2002) and Pope et al (2001). This study will concentrate on looking at the mean over the North Atlantic and North Pacific oceans.

Figures 1 and 2 show the zonal mean U wind errors over the North Atlantic and Pacific for DJF. It is immediately clear from the plots (Fig 1(f) & Fig 2(f)) that the westerly flow across the Atlantic is weaker and located in the mean further north than that over the Pacific. At N48 despite the differences in the flow over the Atlantic and Pacific the model biases are remarkably similar (fig 1(a) & 2(a) i.e. N48L30 has the westerly jet too far equatorward over both oceans. At N96 the mean biases over the Atlantic tend to be smaller than over the North Pacific. Increasing horizontal resolution has moved the westerly jet poleward giving very good agreement with ERA over the North Atlantic but tending to move the jet too far poleward over the Pacific particularly at N96L19. Increasing vertical resolution strengthens the westerly jets and shifts them equatorward. An examination of day 1 spinup tendencies for u (Fig 3) shows some evidence of a shift over the N Atlantic with increasing horizontal resolution. A plot for the Pacific (not shown) shows a similar shift in winds but the shift is further south. This change appears to be due to the dynamics probably due to a thermal wind adjustment due to temperature changes (see later). An examination of the corresponding spinup tendencies for changing vertical resolution shows no evidence of the equatorward shift. This suggests that the equatorward shift in the jets

seen on increasing vertical resolution is not due to a fast process but due to slower more indirect circulation changes.

Figures for temperature (figs 4 and 5) show a similar picture to those for wind, the biases are similar over both oceans at N48 for the upper troposphere and are smaller and different over the oceans at higher resolution. Near the surface (800-1000hPa) at all resolutions over the North Atlantic the model runs show a small warm bias. This warm bias is not present between 30°-60°N over the Pacific. Figure 4 and 5 show the changes in temperature due to changing resolution i.e. increasing horizontal resolution warming the troposphere (fig 4(e) & 5(e)). An examination of spin-up tendencies (Pope and Stratton 2002) also fig 6, suggests that this warming in the region of the storm track is due to increased condensation and dynamics. The condensation increases with resolution because the vertical ascent and descent increases.

Figure 4(b), 4(d), 5(b) & 5(d) show that increasing vertical resolution tends to cool the upper troposphere between 30°-50°N while warming it to the north of this. Looking at spin-up tendencies for increasing vertical resolution at N48 (fig 6) shows a more complex picture. Firstly the spinup tendency changes for increasing vertical resolution do not correspond as clearly with the mean change in temperature making it more difficult to draw conclusions from the spinup tendencies. There is some evidence of cooling around 500hPa (eta =0.5) at ~40°N but this seems to come from a combination of changes to dynamics, cloud, precipitation and radiation. The change in radiation comes from increased longwave cooling, as moisture in the atmosphere is reduced (fig 7). The amount of layer cloud has also reduced. Some of the cooling is partly compensated for by increase heating from convection.

Increasing horizontal resolution tends to increase the moisture in the upper troposphere between 30°-60°N over the Atlantic and Pacific. The lower troposphere dries. The net impact is to leave the Atlantic with a moist bias where the Pacific is too dry compared with ERA. Looking at the spinup tendencies for moisture over the North Atlantic, fig 8, suggests the upper troposphere increase is due to an increased tendency for the dynamics to move moisture upward and not being completely balanced by the increased removal by precipitation. In the lower troposphere (800-600 hPa) the increased removal of moisture by precipitation wins. The increased dry bias in the boundary layer over both oceans at N96 is related to the increased drying by the dynamics not being balanced by an increased moistening from the boundary layer and convection.

On increasing vertical resolution the moisture decreases throughout most of the troposphere. Spinup tendencies suggest this is due to less vertical transport of moisture by dynamics to the upper troposphere and more removal by convection in the mid-troposphere. The increased moisture at low level over the Atlantic may be coming from the boundary layer.

The changes in moisture and cloud mentioned earlier are associated with changes in the precipitation. Figure 9 shows the precipitation for the North Atlantic from the model and from CMAP. The model tends to have more precipitation along the storm track than observed both in the Atlantic and the Pacific (not shown). As vertical resolution increases the proportion of large-scale rainfall decreases and is replaced by convective precipitation. Increasing horizontal resolution leads to an increase in large-scale precipitation coming from the increased condensation mentioned earlier. Convection precipitation just to the south of this is reduced.

Diabatic heating is important in the development of storms. Changes in precipitation, moisture and temperature suggest this is changing with resolution. One

way to assess the diabatic heating of the model against ERA data is to use pressure data and the residual calculation (Hoskins et al 1989). Figure 10 shows a meridional section of diabatic heating across the Pacific. The diabatic heating is too high relative to ERA for the mid-troposphere and too low in the boundary layer (this is also true over the Atlantic although not at the start of the storm track). Changing horizontal resolution does not significantly alter these model biases. The runs with only 19 levels give better agreement with ERA as the diabatic heating in the mid-troposphere is reduced slightly.

Increasing vertical resolution tends to increase the diabatic heating between 30°-45°N, due to more convection, while decreasing the heating further north. Increasing horizontal resolution tends to decrease the heating between 30°-45°N and increase it further north. As the model temperature does not change dramatically with resolution, changes to the diabatic heating will tend to be balanced by opposite changes to the adiabatic heating. The changes tend to correspond to the shift seen in the storm track i.e. as horizontal resolution increases the track shifts poleward and the diabatic heating shifts poleward.

4.2 Baroclinicity and the Eady parameter

The Eady parameter is largest at the beginning of the storm tracks (figure 11 ERA DJF NH). This is consistent with the diabatic heating being large and the atmosphere less stable. Values for ERA and NCEP (not shown) at 500 hPa for DJF 1979-93 are in good agreement.

Comparison of the model with ERA shows that the model integrations at all resolutions tend to have too high a value for the Eady parameter towards the end of the Pacific storm track. This is probably due more to errors in the mean vertical temperature gradient rather than errors in the vertical wind gradient. In the North Atlantic the model tends to lack baroclinicity at the start of the storms track over New Foundland but have too much towards the end.

Increasing vertical resolution tends to increase the excessive baroclinicity at the end of the Pacific storm track. This change is consistent with the overall increase in mean precipitation (more convective) towards the end of the Pacific storm track. The high baroclinicity at the beginning of the Atlantic track is shifted to the south consistent with the general equatorward shift of the westerly jets with vertical resolution.

Increasing horizontal resolution tends to reduce the Eady parameter at the end of the Pacific storm track. There is a large decrease in the convective rainfall at the end of the Pacific storm track with less of an increase in large-scale precipitation indicating a more stable atmosphere. The error at the start of the Atlantic storm track is reduced with higher horizontal resolution.

4.3 Band pass filtered fields

4.3.1 500 hPa heights

The standard deviation of band pass filtered 500hPa heights is commonly used to look at storm tracks providing a mid-tropospheric measure of the variability. The values are largest towards the beginning of the storms tracks, fig 12(f). At all resolutions in DJF the model tends to lack storm activity in the region between Greenland and Iceland and near New Foundland, figure 12(e). Increasing vertical resolution tends to reduce the Atlantic storm track and at N96 shift it equatorward. In the Pacific increasing vertical resolution weakens the storm track and shifts it equatorward, the exact location of the shift depending whether the model is N48

(~150°E) or N96 (~180°E). Increasing horizontal resolution tends to strength the storm track particularly in the Atlantic and also shifts it poleward. The end of Atlantic storm track is extended providing much better agreement with ERA. The net impact of increasing both vertical and horizontal resolution is to improve agreement with ERA, the best agreement at N144L30 (not shown). Similar impacts are seen in the Southern Hemisphere storm track on changing resolution again leading to improvements with ERA.

4.3.2 700hPa v'T' and 200hPa E-vectors.

Study of the mean diabatic heating in the model suggests they may be problems in the region of the storm tracks and that heating may change with resolution. This section looks at the heat transport by cyclonic eddies by looking at the Northward eddy heat transport (v'T') at 700 hPa. Northward eddy heat transport like baroclinicity is largest at the beginning of the storm track, Fig 13. Later on in the development of a storm and higher in the troposphere the eddies transport momentum which can be studied by looking at E vectors (also shown in fig 13).

At all resolutions except N96L19 the model lacks transient poleward heat flux off New Foundland and just north of Iceland. This is consistent with the lack of strength in the Atlantic storm track seen the in 500hPa. Towards the end of the Pacific storm track the model v'T' is too high relative to ERA suggesting that the model may tend to develop too many storms in this region. As vertical resolution is increased v'T' at 700hPa decreases particularly over the middle of the North Atlantic and middle of North Pacific as does the upwards flux of eddy heat transport (w'T') at 700hPa. Increasing horizontal resolution increases v'T' at the beginning of the Atlantic storm track and over the middle of the North Pacific both changes improving agreement with ERA.

Given there are problems with eddy heat transport indicating problems with the development of the storms it is not surprising that there are also problems with the E-vectors at 200 hPa. At all resolutions the E-vectors over the end of the Pacific storm track are too strong. Increasing vertical resolution tends to reduce the strength of the E-vectors at the end of the Atlantic and Pacific storm tracks. Increasing horizontal resolution reduces the E-vectors even further particularly across the USA improving agreement with ERA.

4.3.3 Band pass filtered eddy transport of moisture

In the lower to mid troposphere storms transport moisture both upwards and poleward. Fig 14 shows the northward eddy transport of moisture at 700 hPa. The pattern of biases is very similar at 500 hPa. At all resolution there is too much moisture transport at the end of the Pacific storm track. Looking at w'q', there is also evidence that there is too much vertical transport of water by the eddies at the end of the Pacific storm track. The impact of changing resolution on the transport of moisture by the eddies is very similar to that seen for the eddy heat transport, increasing vertical resolution reduces the eddy transport at the beginning of the North Atlantic storm track, increasing horizontal resolution increases eddy transport.

Over the Atlantic there are differences between the heat and moisture errors particularly at 19 levels. The 19 level models tend to transport too much moisture northwards at the beginning of the N Atlantic storm track but not enough heat in the eddies. The excessive transport of moisture may be related to the mean moist bias of the model over the Atlantic, Fig 7 where as the model mean is drier over the Pacific.

4.4 Feature tracking analysis

The feature tracking analysis in this study only looks at mean sea level pressure and so concentrates on the surface features of the storms. The previous sections tended to concentrate on the characteristics of the storms in the lower and mid-troposphere. This may explain why some of the results from the feature analysis differ from the band pass filtered analysis.

4.4.1 Northern Hemisphere DJF

Strength and track density

The plots of track density (Fig 15) show an equatorward shift in the track density on increasing vertical resolution consistent with the shift in the westerly winds. Increasing horizontal resolution gives the reverse i.e. a poleward shift in the storm track again consistent with the shift in the mean westerly winds. These changes agree with those found from looking at band passed filtered 500hPa heights.

The mean peak strength of cyclones in the Pacific and Atlantic decreases with increasing horizontal resolution (Fig 16). This at first appears inconsistent with the track density and 500hPa band pass filtered heights results which show a poleward shift and an increase but track strength is a different measure to density and height variability. The results are consistent with the change in the mean sea level pressure for DJF in the region of the storm tracks. This increases with increasing resolution. It is difficult to see any clear change in cyclone strength on increasing vertical resolution.

Speed

Speed of cyclones over most of the Pacific decrease with horizontal resolution, fig 17, while the peak speed at around 160-170E increases with horizontal resolution, both changes improving agreement with ERA. These changes are consistent with the easterly jet moving poleward and decreasing in strength with increasing horizontal resolution and the 200hPa E vectors decreasing. In the Atlantic towards the beginning of the storm track the reverse is true, speed increases with horizontal resolution. Again this change is consistent with the upper level change in the westerly jet.

There is also evidence that increasing vertical resolution leads to an increase in speed towards the eastern end if the Pacific storm track which is detrimental.

Growth, decay and lifetime.

Cyclones grow quickly over the eastern states of the USA and the Western part of both the Atlantic and Pacific. The model simulations seem to capture the general characteristics of cyclone growth and decay. Growth of cyclones over the southern end of the Rockies increases with increasing vertical resolution but decreases with horizontal resolution (fig 18). Similarly decay rates between Greenland and Canada increase with horizontal resolution and decrease with increasing vertical resolution. There is some evidence that at lower horizontal resolution cyclones grow more quickly over the mid-Pacific. This does not improve agreement with ERA but is consistent with the excessive northwards eddy heat transport at N48.

Cyclones at N48 tend to have longer lifetimes (by approximately 1 day) than those at N96 (Fig 19) over both the Pacific and Atlantic. One possible reason for this is that at higher resolution more secondary cyclogenesis occurs mid-Pacific and mid-Atlantic i.e. the cyclones at the beginning of the storm track do not travel right across

the oceans see investigation in the next section. However, even at N96 the mean lifetime of the cyclones is too long by the order of 1-1.5 days.

Cyclo-genesis and lysis

Overall the regions of cyclo-genesis (fig 20) are similar at all resolutions and it is difficult to detect strong signals in the differences. One difference occurs just south of the Great Lakes, with 19 levels there is more cyclo-genesis than with 30 levels. Just down stream of this off the coast of the USA there is more cyclo-genesis with 30 levels. At lower horizontal resolution there is a second area of strong spurious cyclo-genesis North of the Himalayas. The lysis density (fig 21) shows similar systematic errors at all resolutions with spurious cyclones created over Asia decaying over Eastern Asia.

Looking at the cyclo-genesis plots it is hard to find any evidence that increasing resolution increases secondary cyclo-genesis in the middle of the Pacific. Overall there is a slight reduction in cyclo-genesis density over the Pacific with increasing horizontal resoltuion. Lysis density is higher at N96 suggesting more cyclones are dying at higher horizontal resolution in mid-Pacific thus contributing to the shorter lifetimes at higher resolution.

Increasing vertical resolution gives a slight increase in cyclo-genesis over the Pacific but little change in the lysis density.

Overall the implication of the results are that surface cyclones at N48 tend to be deeper and last longer and are probably less realistic. At N96 with 4 times the number of grid boxes a cyclone can be resolved over a smaller scale and appears to be able to develop and, particularly, to decay more quickly but still not quickly enough to agree with ERA.

Conclusions

The results from this study suggest that increasing horizontal resolution improves the ability of the model to simulate storms. This leads to improvements in both the mean fields and more importantly to the variability as measured on the timescales of storm activity.

Increasing horizontal resolution shifts the storm tracks poleward and increases their strength. The shift in location is linked to the changes in tropospheric heating, which is in turn linked to more vigorous ascent and descent due to better resolution of cyclones. At higher horizontal resolution cyclones decay on more realistic timescales where as at lower resolution the cyclones live longer.

Increasing vertical resolution weakens and shifts the storm tracks equatorward. The causes of these changes are less easy to understand. The vertical transport of moisture improves with increasing vertical resolution and may account for the reduction in mid- to higher level cloud and the changes in outgoing longwave radiation. Work on increasing vertical resolution from 19 to 30 levels (Pope et al 2001) showed that the behaviour of the model's convection scheme is sensitive to the position and number of model levels. At mid-latitudes over the oceans although convection does not dominate the behaviour of the model as in the tropics it is still an important factor. In HadAM3 increasing vertical resolution increases the convective activity in the storm tracks. The detrimental impact of increasing vertical resolution on the representation of the storm tracks in this model requires a better understanding of the role of convection in the storm tracks and the vertical resolution sensitivity of the model.

References

Doblas-Reyes F J and Deque M (1998) A flexible bandpass filtering procedure applied to midlatitude intraseasonal variability. Mon Wea Rev 126: 3326-3335.
Gates W L, Boyle J S, Covey C, Dease C G, Doutriaux C M, Drach R S , Fiorino M, Gleckler P J, Hnilo J J, Marlias S M, Phillips T J, Potter G L, Santer B D, Sperber K R, Taylor K E, Williams D N (1999) An overview of the results of the Atmospheric Model Intercomparison Project (AMIP I). Bull Am Meteorol Soc 80: 29-55.
Gibson K J, Kallberg P, Uppala S, Nomura A, Hernandez A, Serrano E (1997) ERA description, ECMWF re-anlaysis project report series 1, ECMWF, Reading, UK.
Hoskins B J, James I N and White G H (1983) The Shape, propagation and mean-flow interaction of large-scale weather systems. J Atm Sci 40: 1595-1612.
Hoskins B J, Hsu H H, James I N, Matsutani M, Sardeshmukh P H and White G H (1989) Diagnostics of the global atmospheric circulation, based on ECMWF analyses 1979-1989. WMO/TD 326, 217pp, Department of Meteorology, University of Reading, Reading UK.
Hoskins B J and Hodges K I (2002) New perspectives on the Northern Hemisphere winter storm tracks. J Atmos Sci 59: 1041-1061.
Hoskins B J and Valdes P J (1990) On the existence of storm tracks. J Atmos Sci 47: 1854-1864.
Kalnay E, Kanamitsu M, Kistler R, Collins W, Deaven D, Gandin L, Iredell M Saba S, White G, Woollen J, Zhu Y, Leetmaa A, Reynolds R, Chelliah M, Ebisuzaki W, Higgins W, Janiwiak J, Mo K C, Popelewski C, Wang J Jenne R, Jospeh D (1996) The NCEP/NCAR 40 year reanalysis project. Bull Am. Met Soc 77: 437-471.
Lindzen R S and Farrell B (1980) A simple approximate results for the maximum growth rate of baroclinic instabilities. J Atmos Sci 37: 1648-1654.
Lindzen R S and Fox-Rabinovitz M (1989) Consistent vertical and horizontal resolution. Mon Wea Rev 117: 2575-2583.
Pope V D, Gallani M L, Rowntree P R and Stratton R A (2000) The impact of new physical parametrizations in the Hadley Centre climate model Had AM3. Clim Dyn 16:123-146.
Pope V D, Pamment J A, Jackson D R, Slingo A (2001) The representation of water vapour and its dependence on vertical resolution in the Hadley Centre climate model. J Clim 14: 3065-3085.
Pope V D, Stratton R A (2002) The processes governing horizontal resolution sensitivity in a climate model. Clim Dyn 19: 211-236.

List of figures

1. U component of wind for DJF over the North Atlantic (0°-60°W) (a) N48L30 minus ERA, (b) N48L30 minus N48L19, (c) N96L30 minus ERA (d) N96L30 minus N48L19, (e) N96L30 minus N48L30, (f) ERA.
2. Same as fig 1 for the North Pacific 140°-230°E.
3. Cross sections of U tendencies for the North Atlantic 0°-60°W.
4. Cross section of mean temperature for DJF over the North Atlantic (0°-60°W) same format as Figure 1.
5. As fig 4 but for North Pacific.
6. Temperature tendency cross-sections for the North Pacific.
7. Cross-sections of specific humidity for the North Atlantic same format as figure 1.
8. Specific humidity tendencies for the North Atlantic 0°-60°W.

9. Precipitation for the North Atlantic.
10. Meridional sections of Diabatic heating for the North Pacific 30°-60°N.
11. Northern hemisphere Eady parameter (a) N96L30 -ERA (b) N48L30 – ERA (c) N96L19 –ERA (d) N48L19 – ERA (e) ERA.
12. Northern Hemisphere band pass filtered 500 hPa heights for DJF (a) N96L30 minus N96L19, (b) N48L30 minus N48L19, (c) N96L30 minus N48L30, (d) N96L19 minus N48L19, (e) N96L39 minus ERA, (f) ERA.
13. V'T' at 700hPa with E vectors at 200 hPA for DJF (a) N96L30, (b) N48L30, (c) N96L19, (d) N48L19, (e) ERA and (f) N96L30 minus ERA.
14. Band pass filtered v'q' for Northern Hemisphere DJF.
15. Storm track density for the Northern Hemisphere DJF (a) N96L30 minus N96L19, (b) N48L30 minus N48L19, (c)N96L30 minus N48L30, (d) N96L19 minus N48L19, (e) N96L30, (f) ERA.
16. Storm track strength for the Northern Hemisphere DJF same format as fig 15.
17. Storm track speed for Northern Hemisphere DJF (a) N96L30, (b) N48L30, (c) N96L19, (d) N48L19, (e) ERA .
18. Storm track growth and decay for Northern Hemisphere DJF same format as 17.
19. Storm track lifetimes for Northern Hemisphere DJF same format as 17.
20. Storm track genesis density for Northern Hemisphere DJF same format as 17.
21. Storm track lysis density for Northern Hemisphere DJF same format as 17.

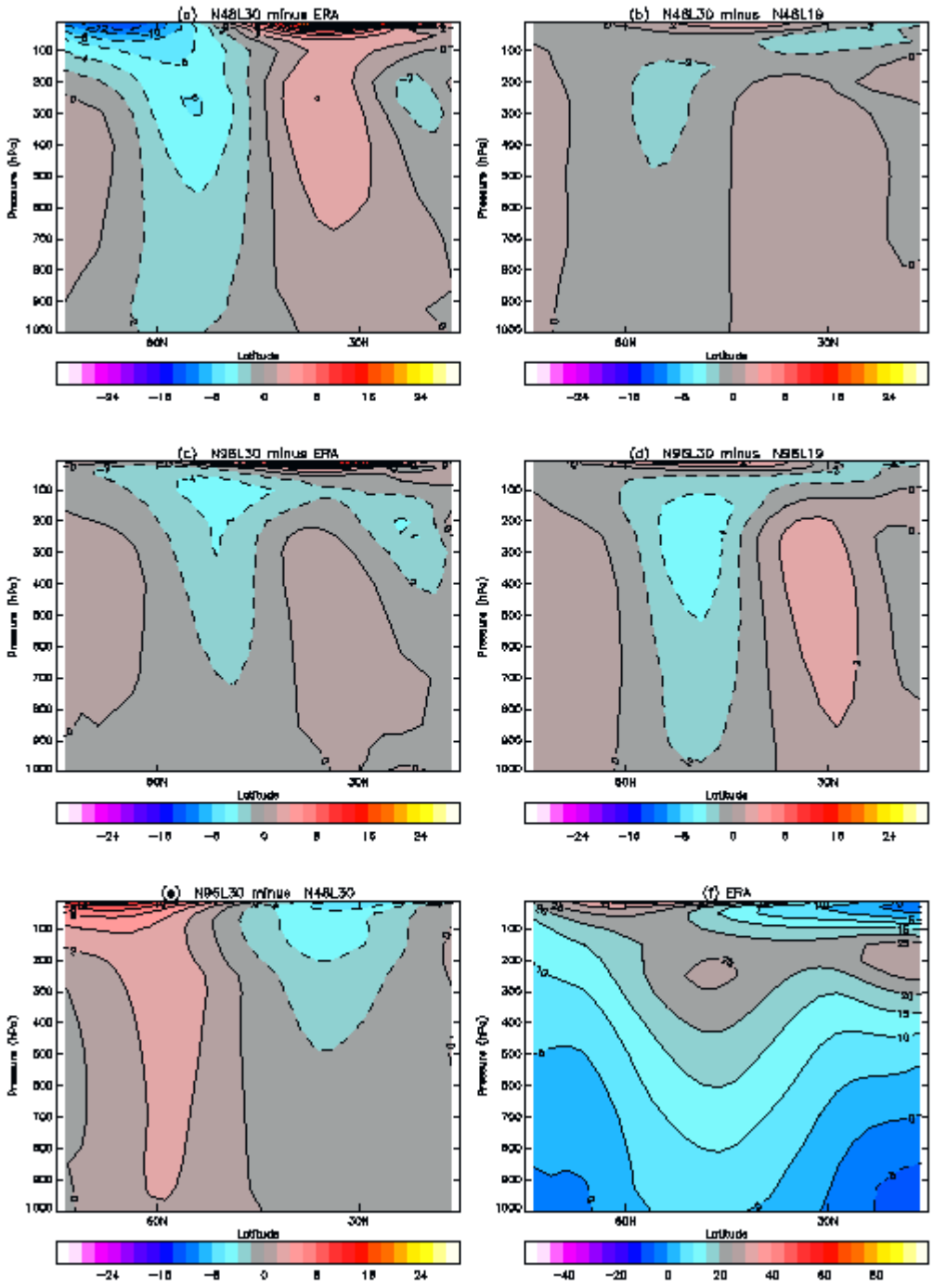
(a) N48L30 minus ERA
(b) N48L30 minus N48L19
(c) N96L30 minus ERA
(d) N96L30 minus N96L19
(e) N96L30 minus N48L30
(f) ERA
Pressure (hPa)
Latitude
60N
30N
−24 −16 −8 0 8 16 24
−40 −20 0 20 40 60 80

Figure 1

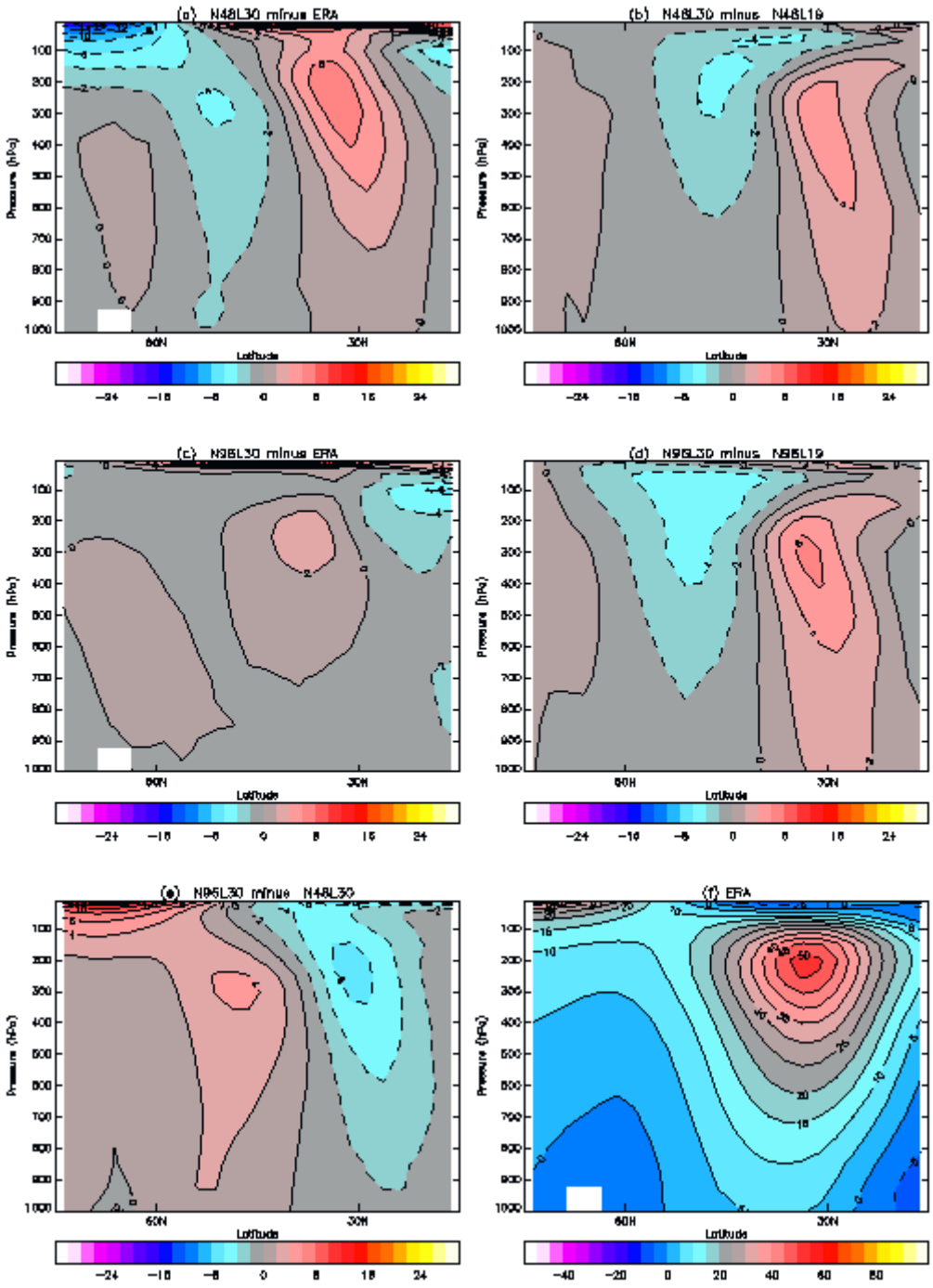
(a) N48L30 minus ERA
(b) N48L30 minus N48L19
(c) N96L30 minus ERA
(d) N96L30 minus N96L19
(e) N96L30 minus N48L30
(f) ERA
Pressure (hPa)
Latitude
60N
30N

Figure 2

Fig 3 U tendency N Atlantic 0–60W

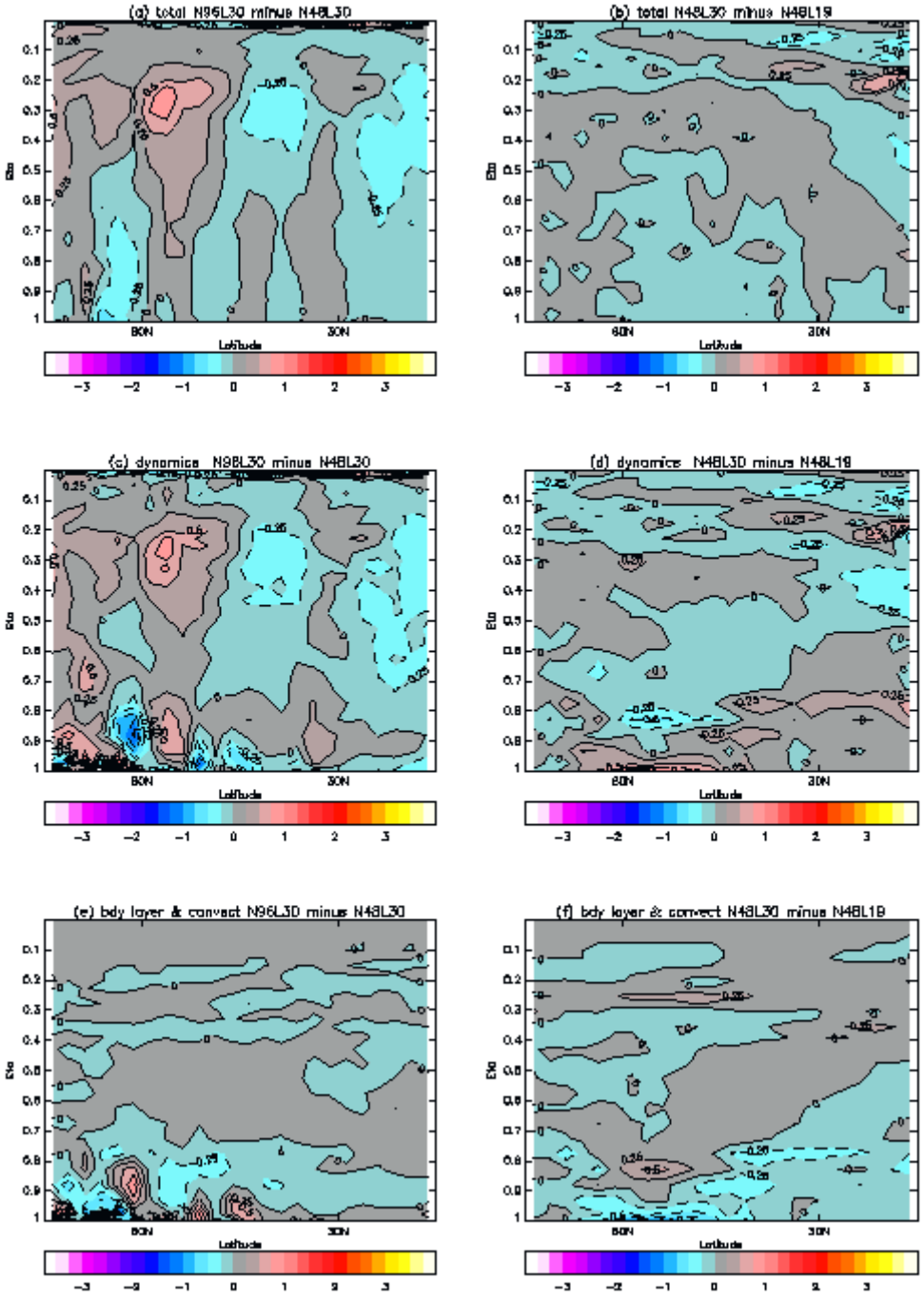

Figure 3

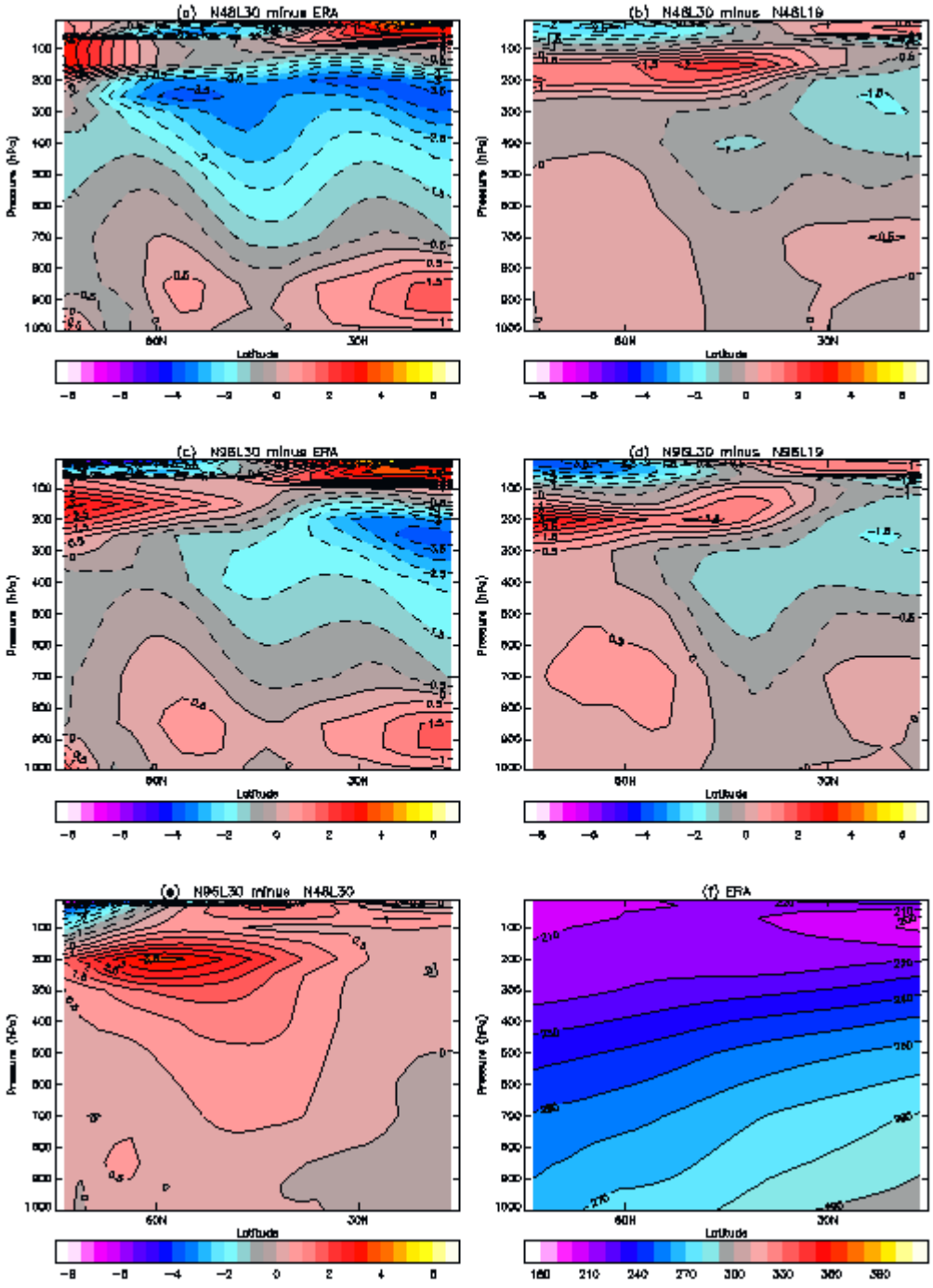
(a) N48L30 minus ERA
(b) N48L30 minus N48L19
(c) N96L30 minus ERA
(d) N96L30 minus N96L19
(e) N96L30 minus N48L30
(f) ERA
Pressure (hPa)
Latitude
60N
30N

Figure 4

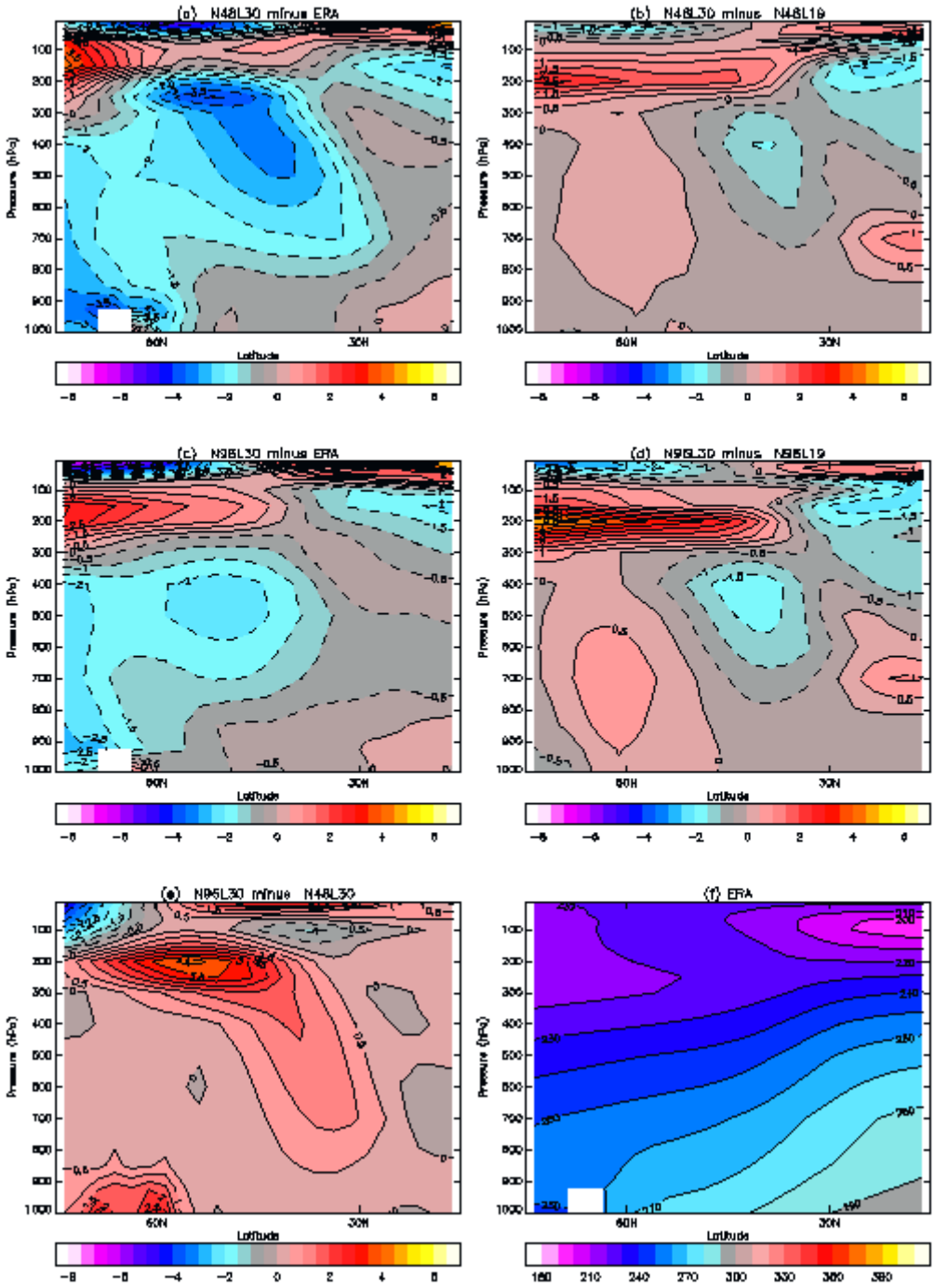
(a) N48L30 minus ERA
(b) N48L30 minus N48L19
(c) N96L30 minus ERA
(d) N96L30 minus N96L19
(e) N96L30 minus N48L30
(f) ERA
Pressure (hPa)
Latitude
60N
30N

Figure 5

Fig 6 T tendency N Atlantic 0–60W

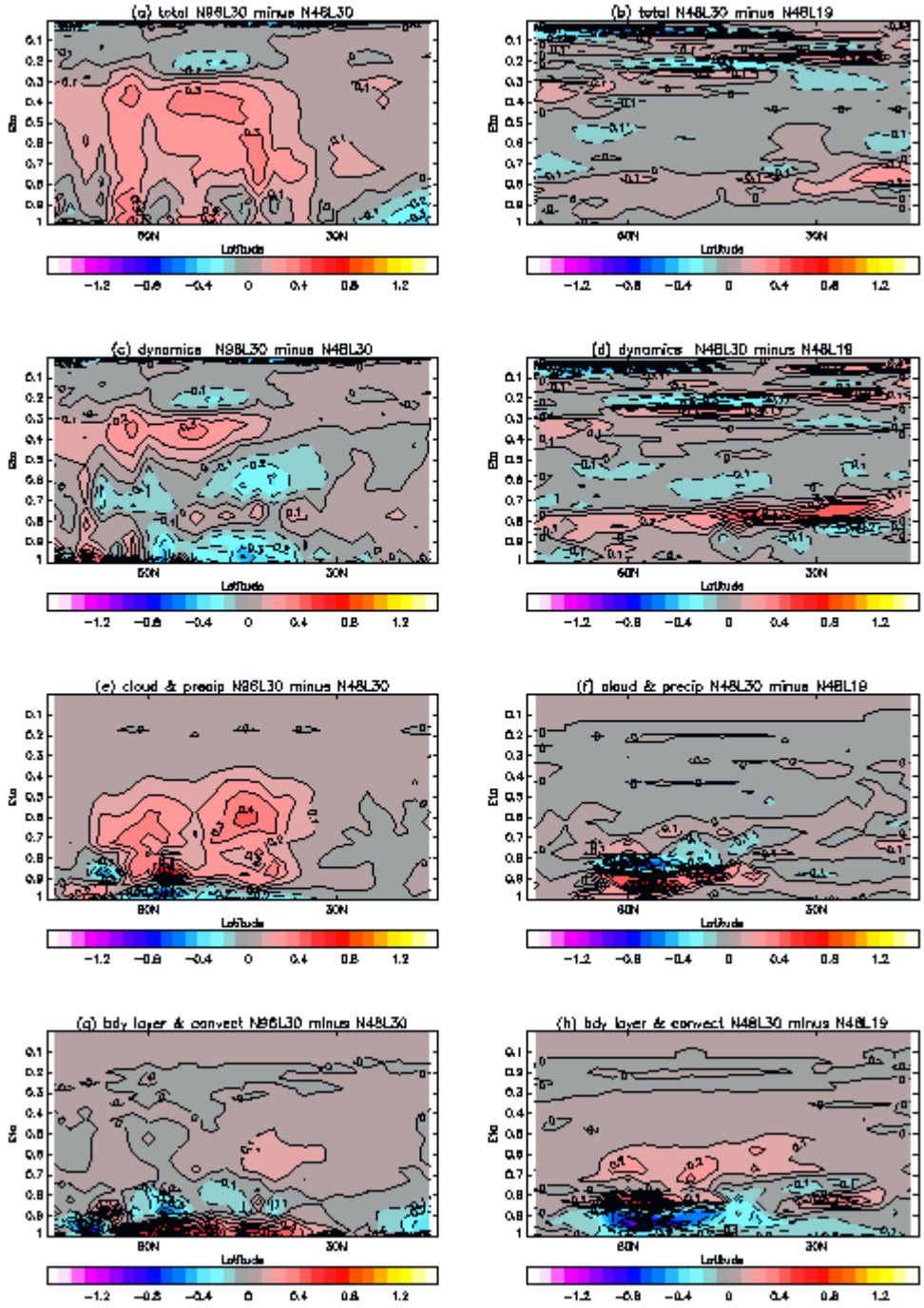

Figure 6

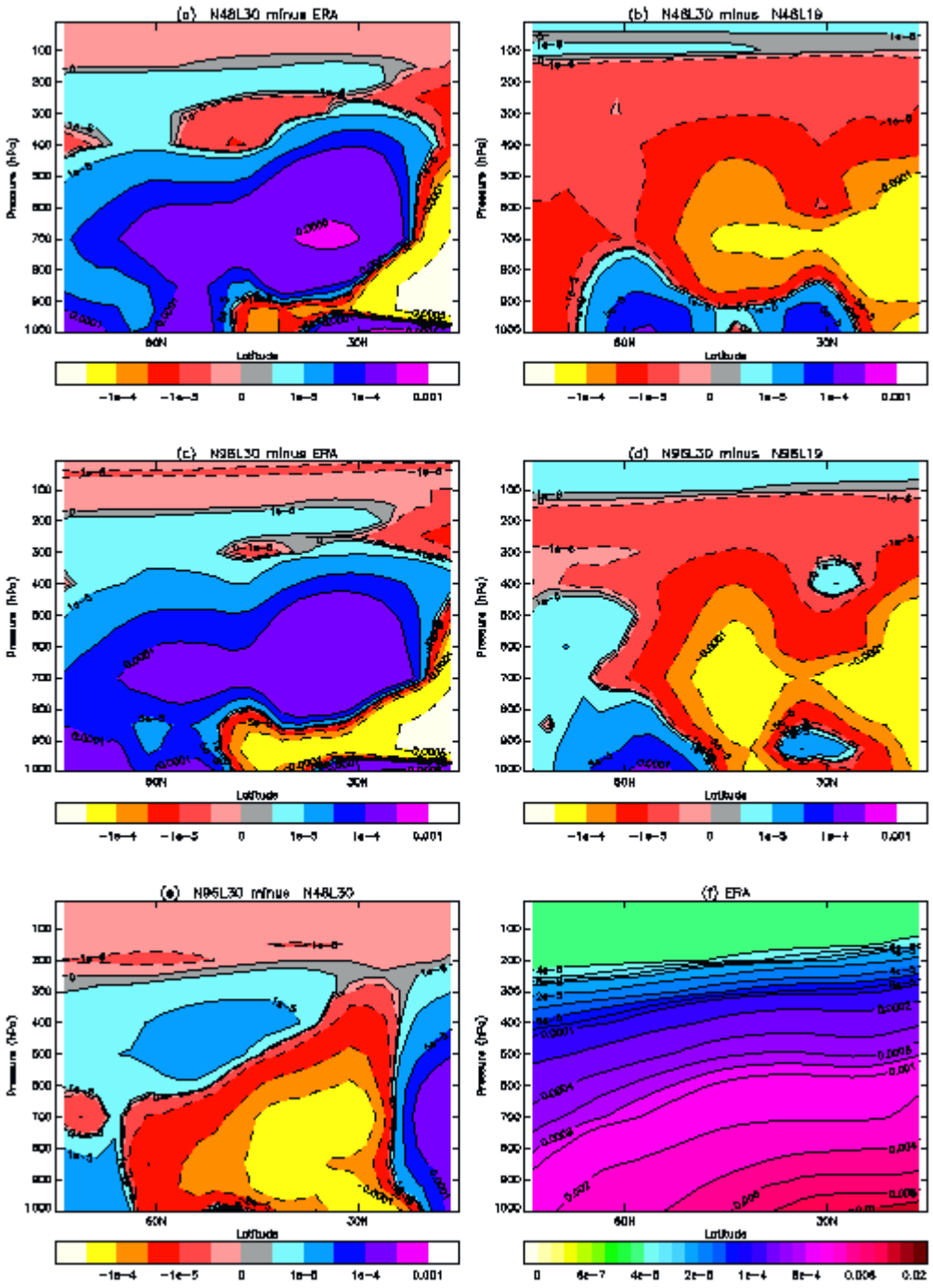
(a) N48L30 minus ERA
(b) N48L30 minus N48L19
(c) N96L30 minus ERA
(d) N96L30 minus N96L19
(e) N96L30 minus N48L30
(f) ERA
Pressure (hPa)
Latitude
60N
30N
−1e−4
−1e−5
0
1e−5
1e−4
0.001
0
6e−7
4e−6
2e−6
1e−4
8e−4
0.006
0.02

Figure 7

Fig 8 q tendency for day 2 N Atlantic 0–60W

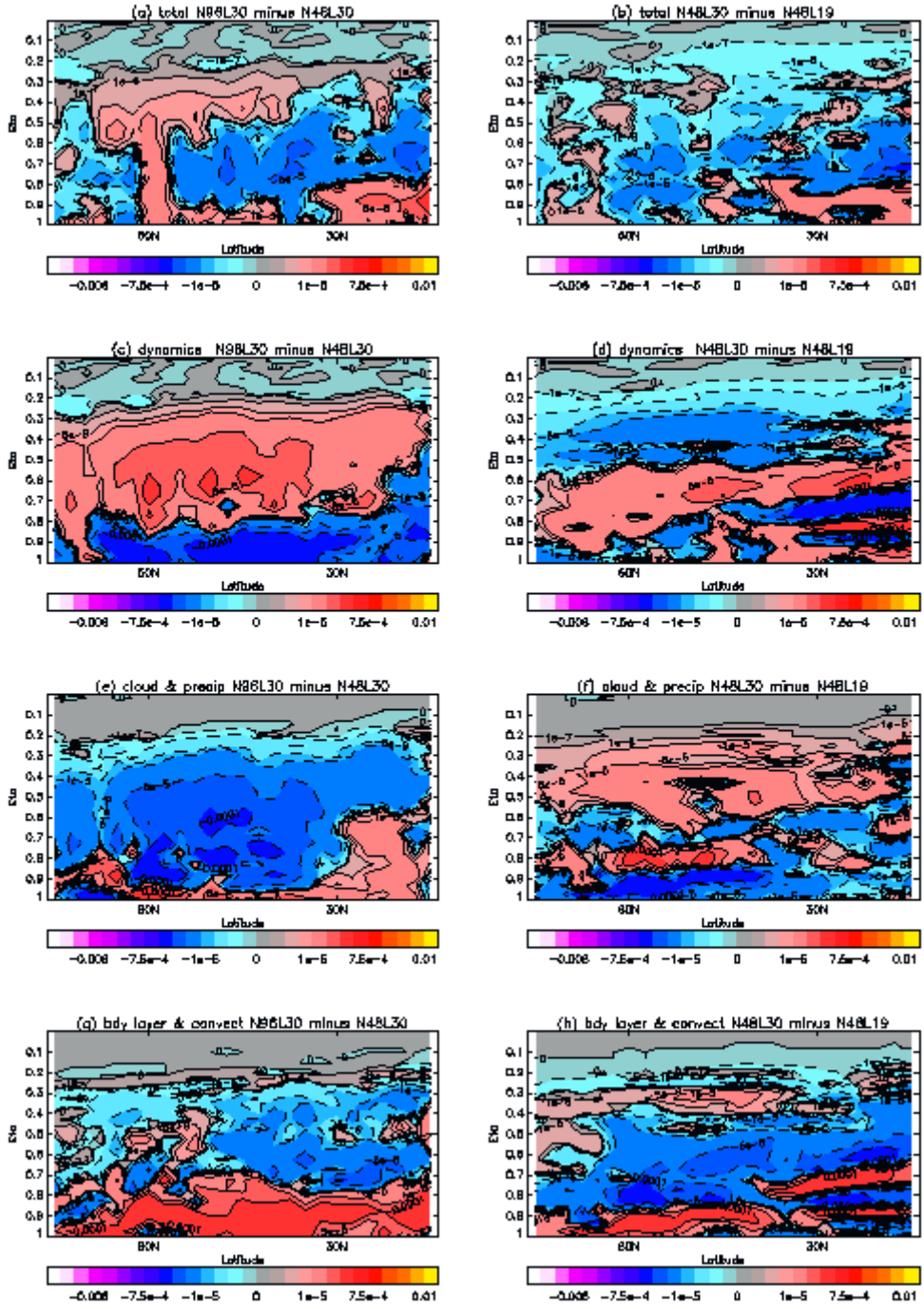

Figure 8

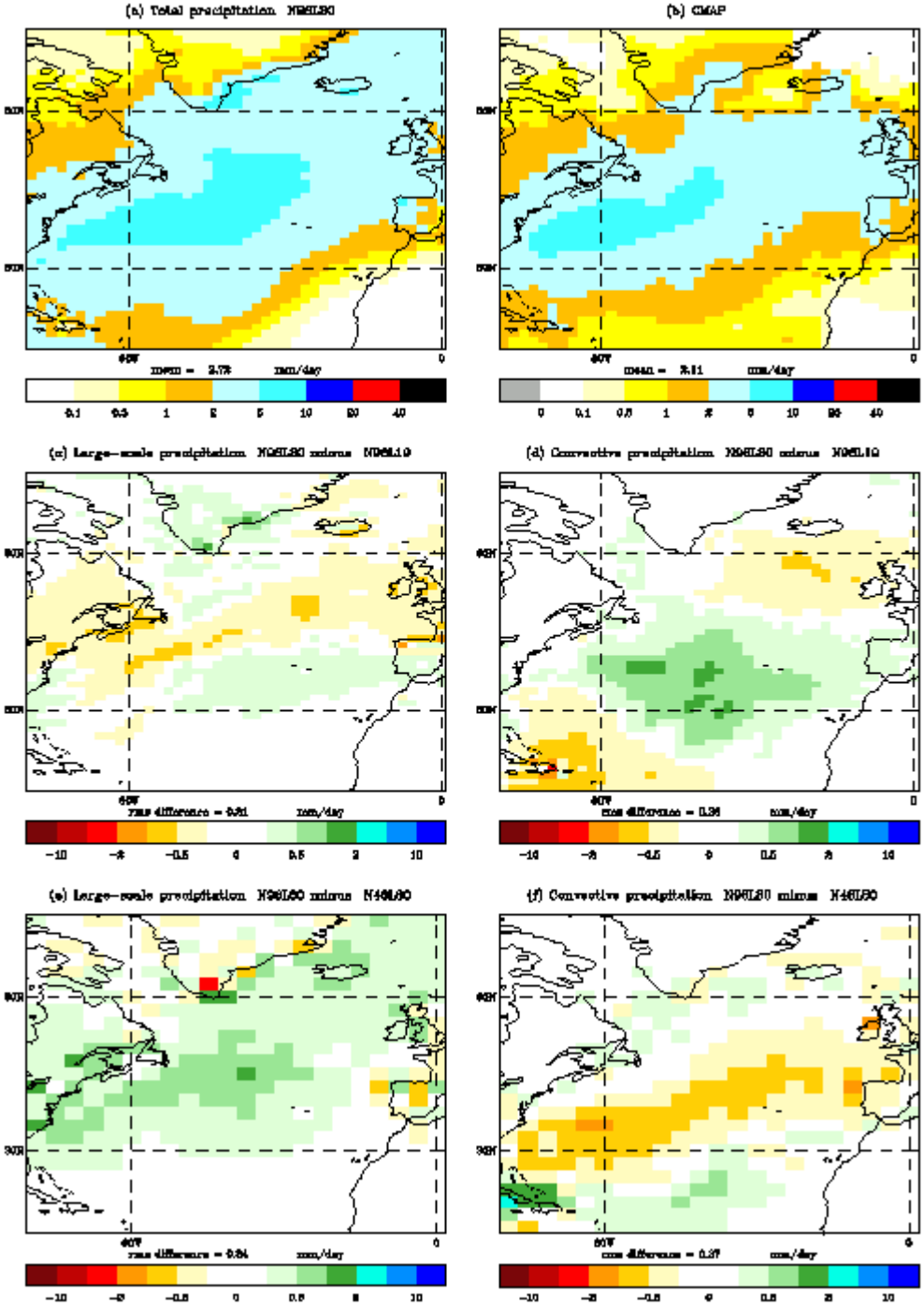
(a) Total precipitation N96L30
(b) CMAP
(c) Large-scale precipitation N96L30 minus N96L19
(d) Convective precipitation N96L30 minus N96L19
(e) Large-scale precipitation N96L30 minus N48L30
(f) Convective precipitation N96L30 minus N48L30

Figure 9

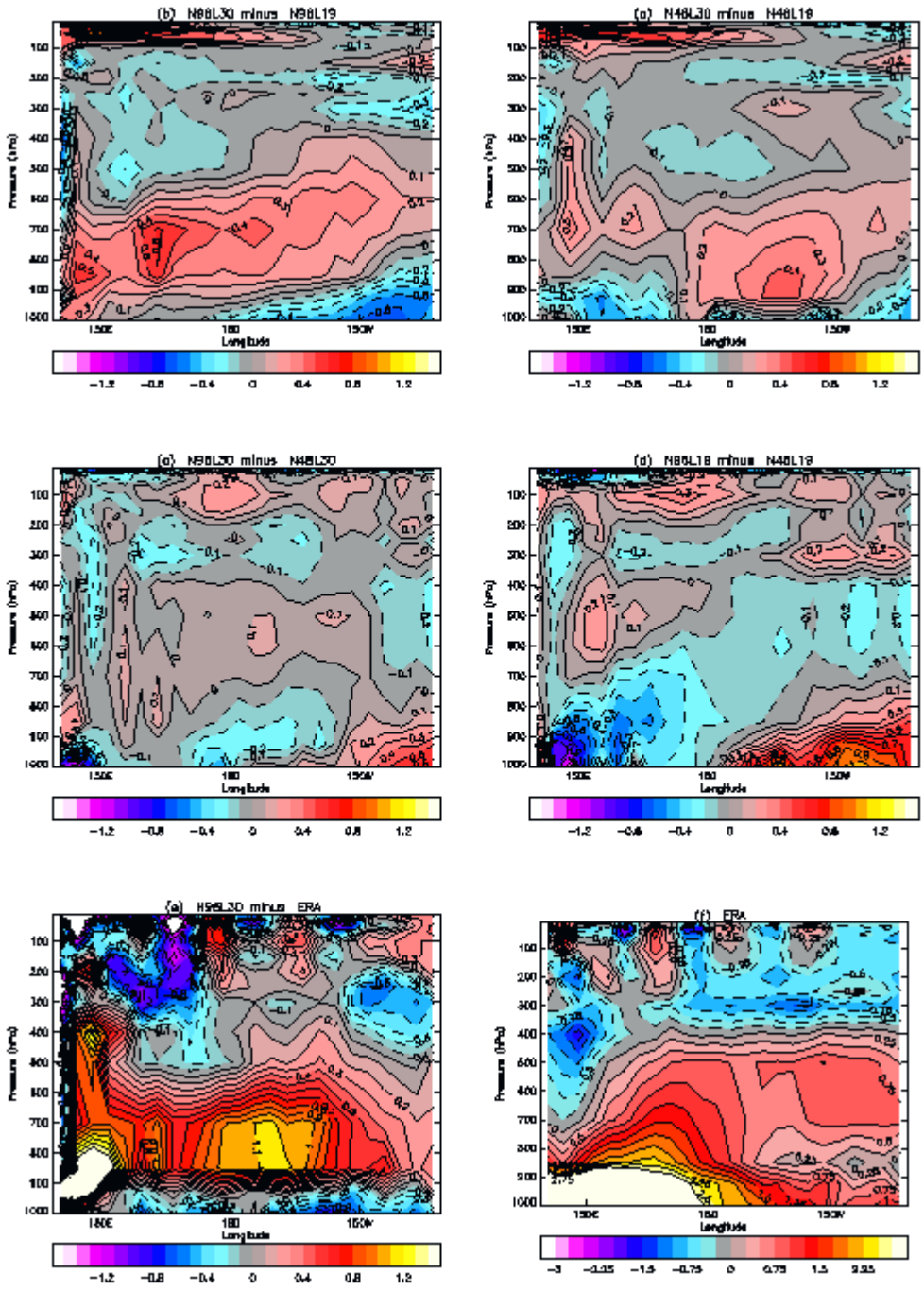
(b) N96L30 minus N96L19
(a) N48L30 minus N48L19
(c) N96L30 minus N48L30
(d) N96L19 minus N48L19
(e) N96L30 minus ERA
(f) ERA
Pressure (hPa)
Longitude
150E
180
150W
−1.2 −0.8 −0.4 0 0.4 0.8 1.2

Figure 10

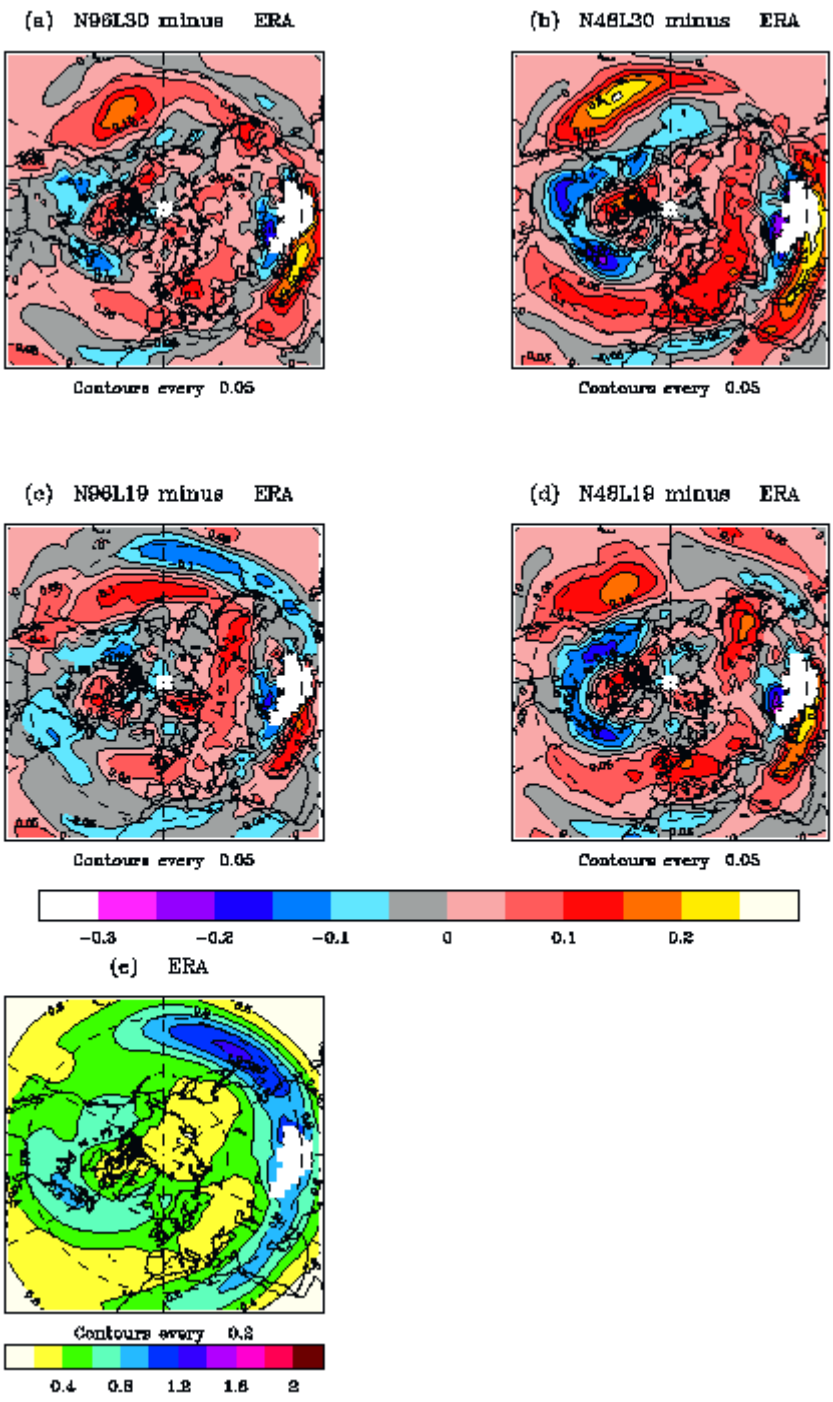
(a) N96L30 minus ERA
Contours every 0.05
(b) N48L30 minus ERA
Contours every 0.05
(c) N96L19 minus ERA
Contours every 0.05
(d) N48L19 minus ERA
Contours every 0.05
−0.3
−0.2
−0.1
0
0.1
0.2
(e) ERA
Contours every 0.2
0.4
0.8
1.2
1.6
2

Figure 11

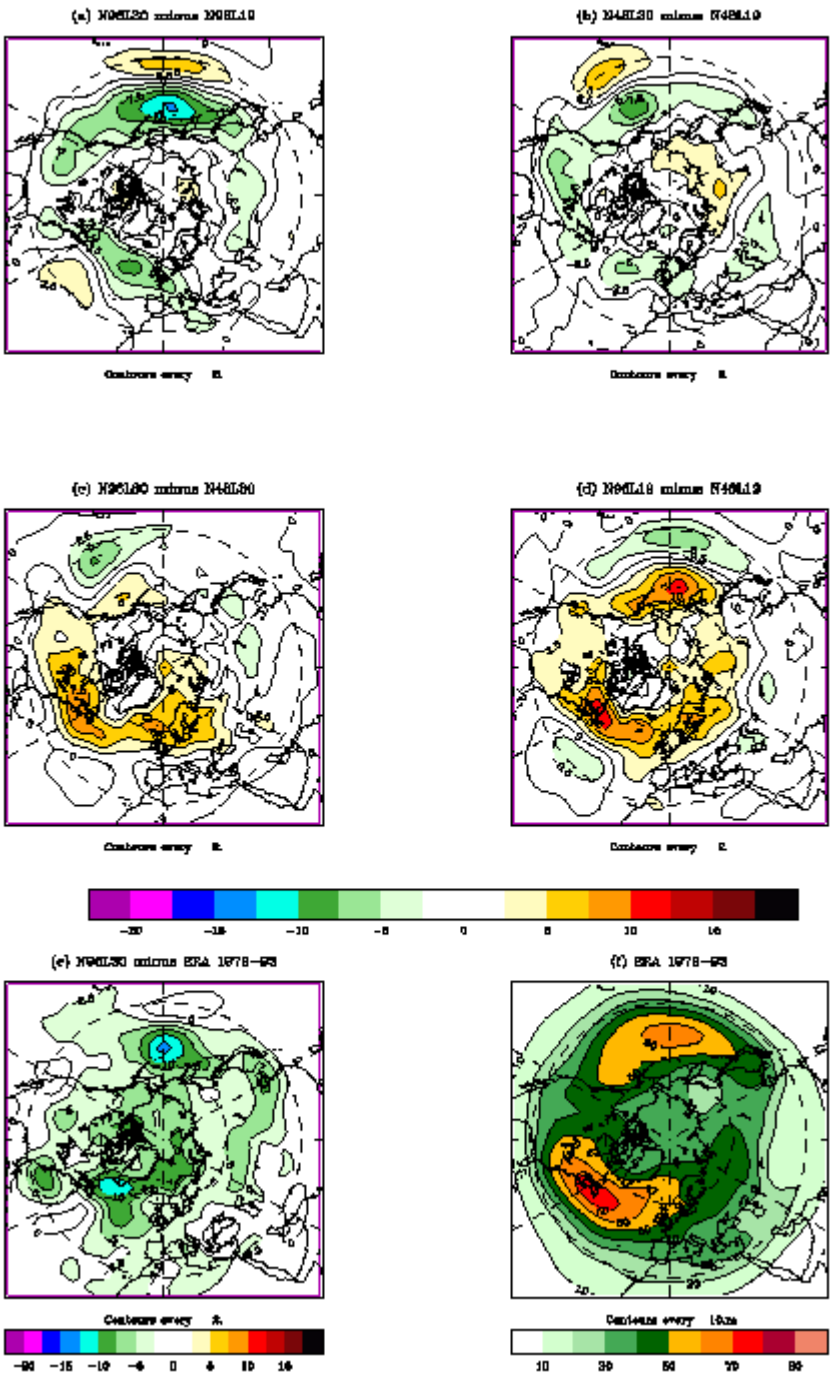

Figure 12

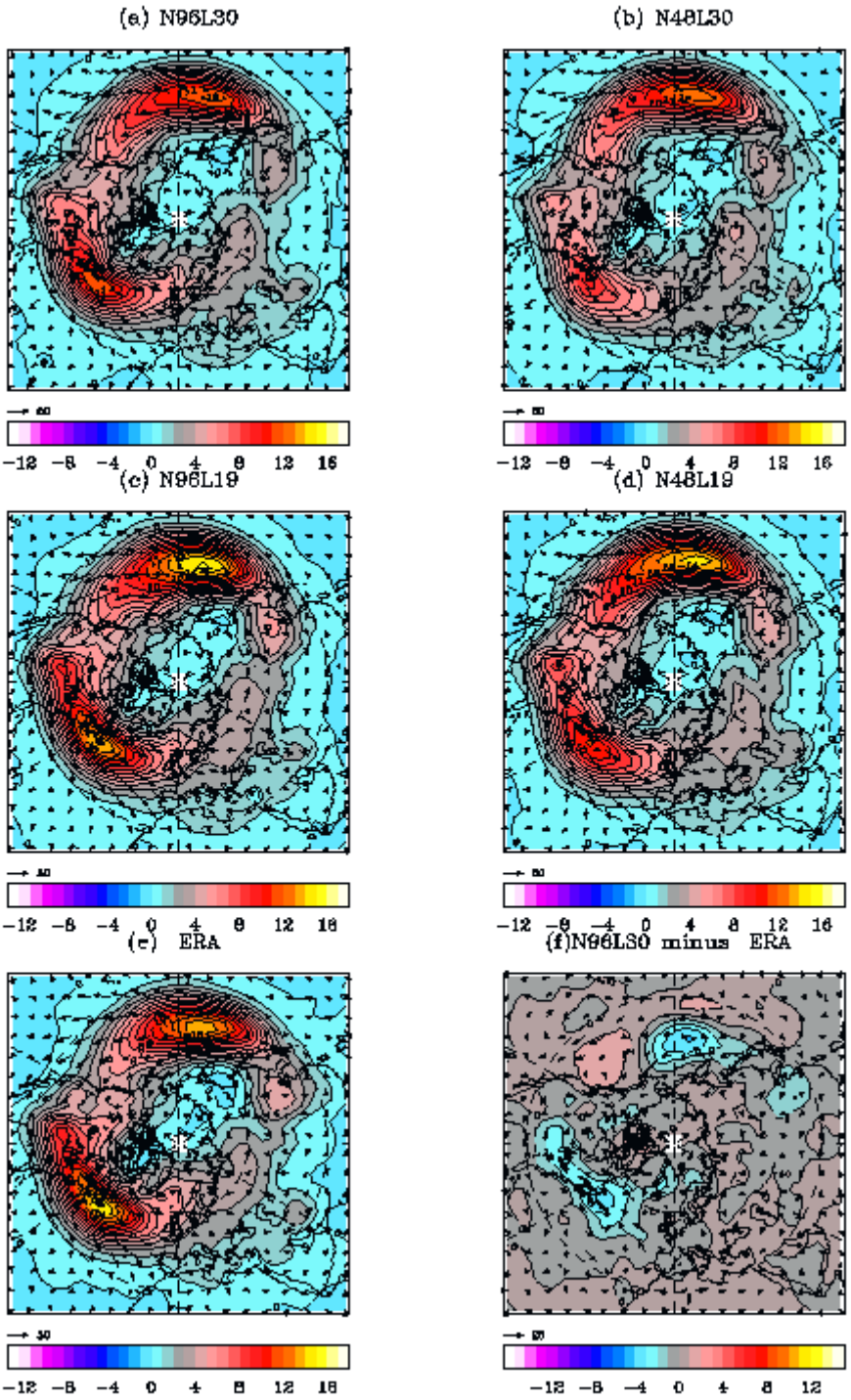
(a) N96L30
(b) N48L30
−12 −8 −4 0 4 8 12 16
(c) N96L19
(d) N48L19
−12 −8 −4 0 4 8 12 16
(e) ERA
(f)N96L30 minus ERA
−12 −8 −4 0 4 8 12 16
−12 −8 −4 0 4 8 12

Figure 13

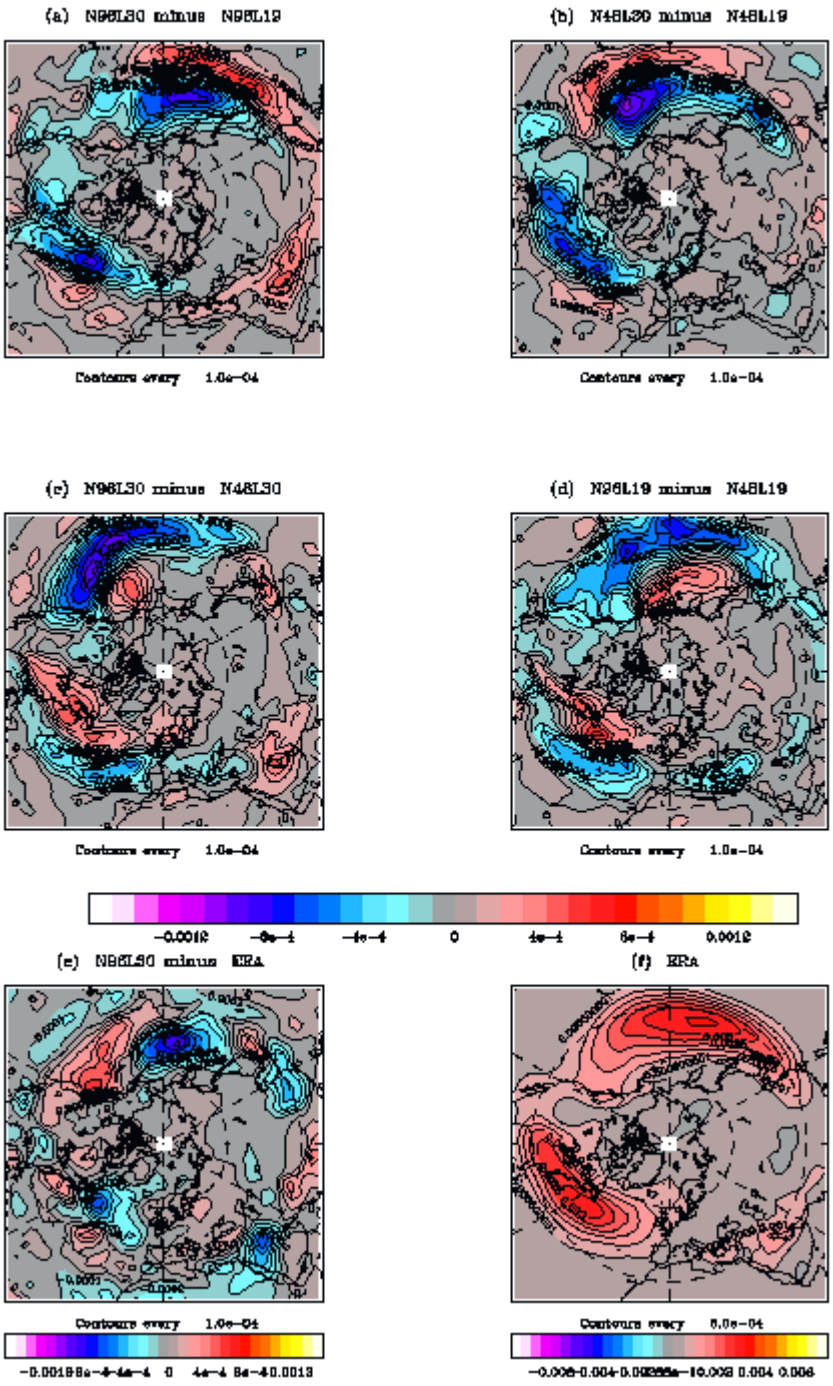
(a) N96L30 minus N96L19
(b) N48L30 minus N48L19
(c) N96L30 minus N48L30
(d) N96L19 minus N48L19
(e) N96L30 minus ERA
(f) ERA

Figure 14

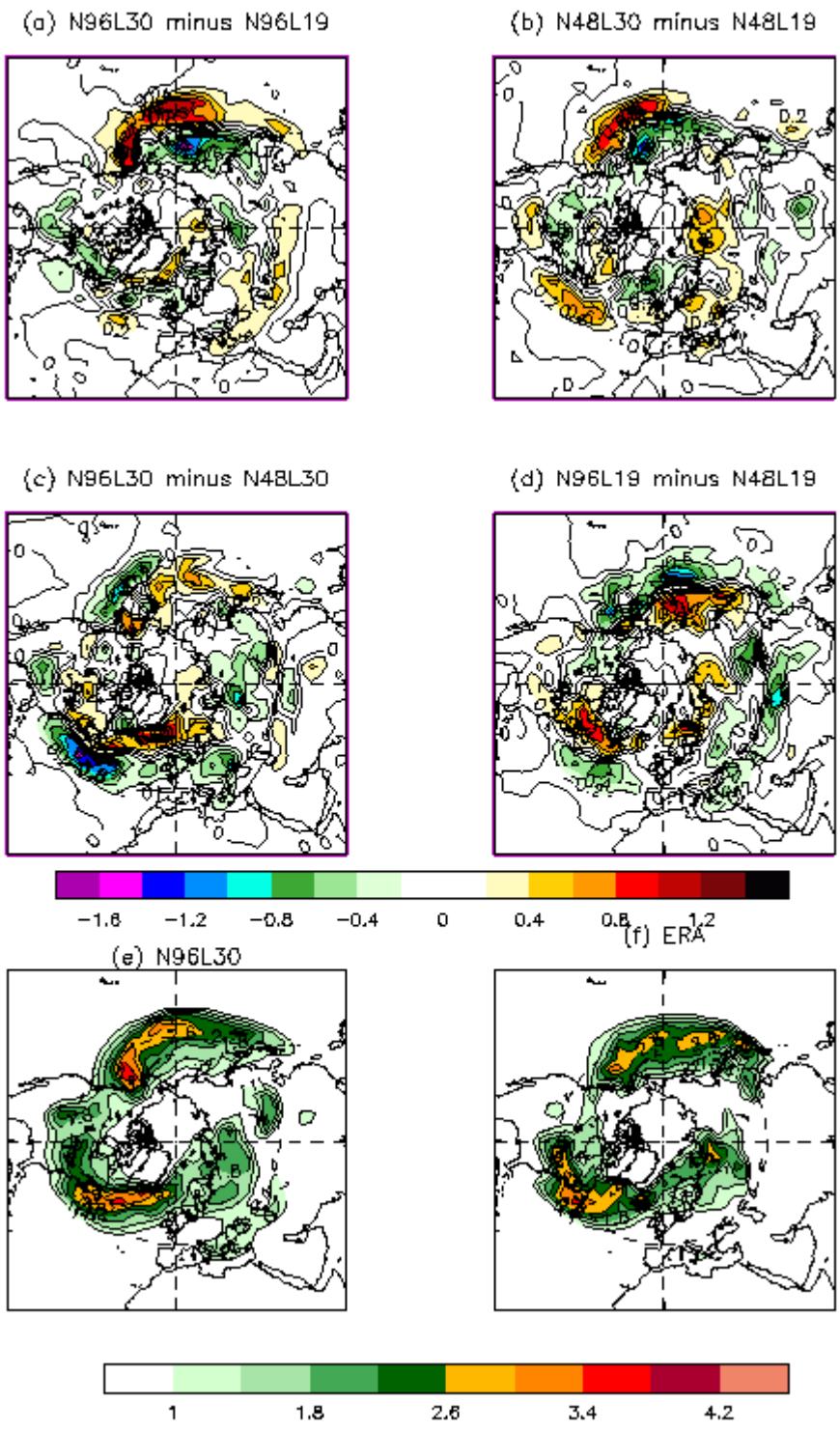
(a) N96L30 minus N96L19
(b) N48L30 minus N48L19
(c) N96L30 minus N48L30
(d) N96L19 minus N48L19
−1.6
−1.2
−0.8
−0.4
0
0.4
0.8
1.2
(e) N96L30
(f) ERA
1
1.8
2.6
3.4
4.2

Figure 15

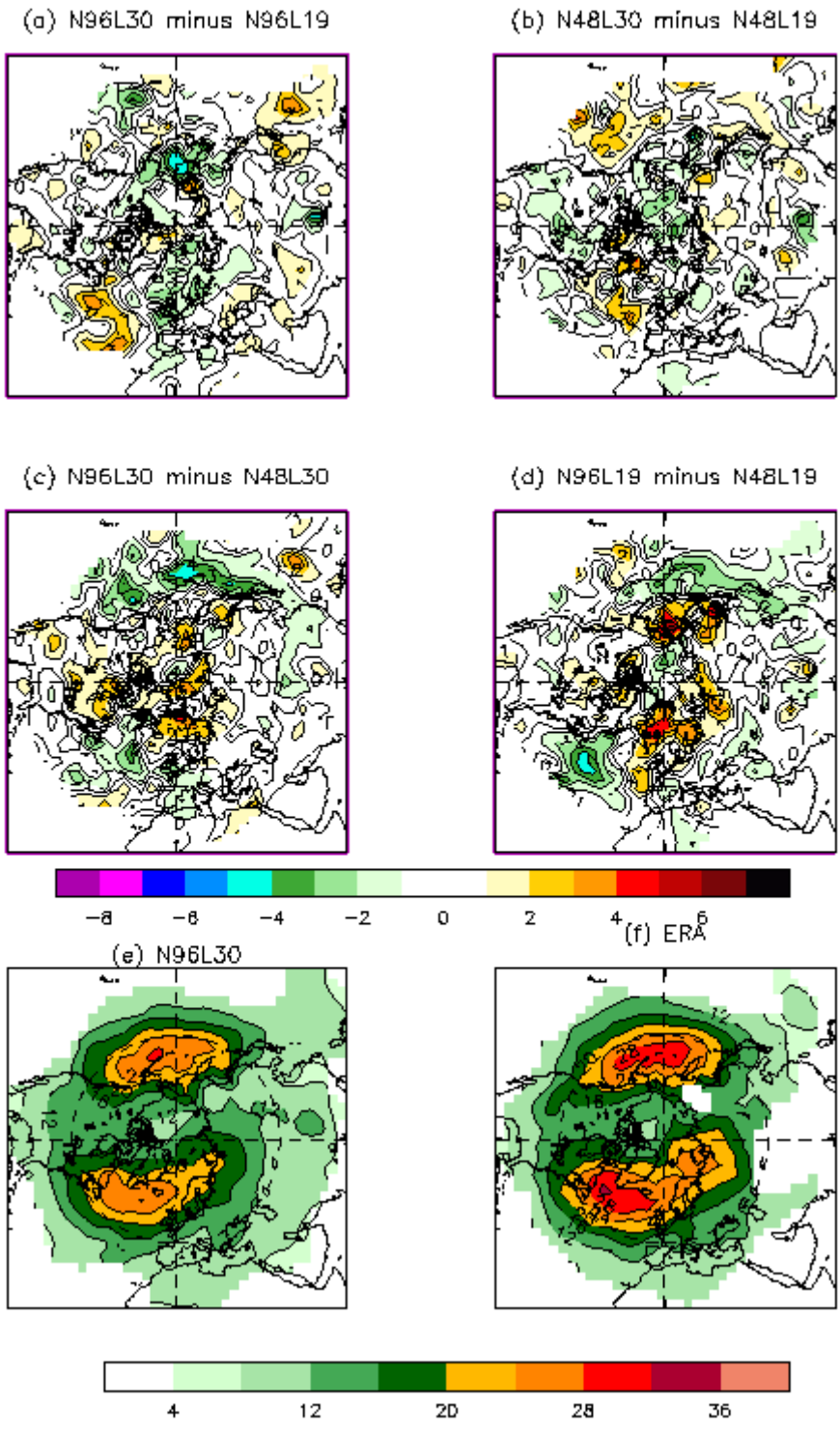
(a) N96L30 minus N96L19
(b) N48L30 minus N48L19
(c) N96L30 minus N48L30
(d) N96L19 minus N48L19
−8
−6
−4
−2
0
2
4
6
(e) N96L30
(f) ERA
4
12
20
28
36

Figure 16

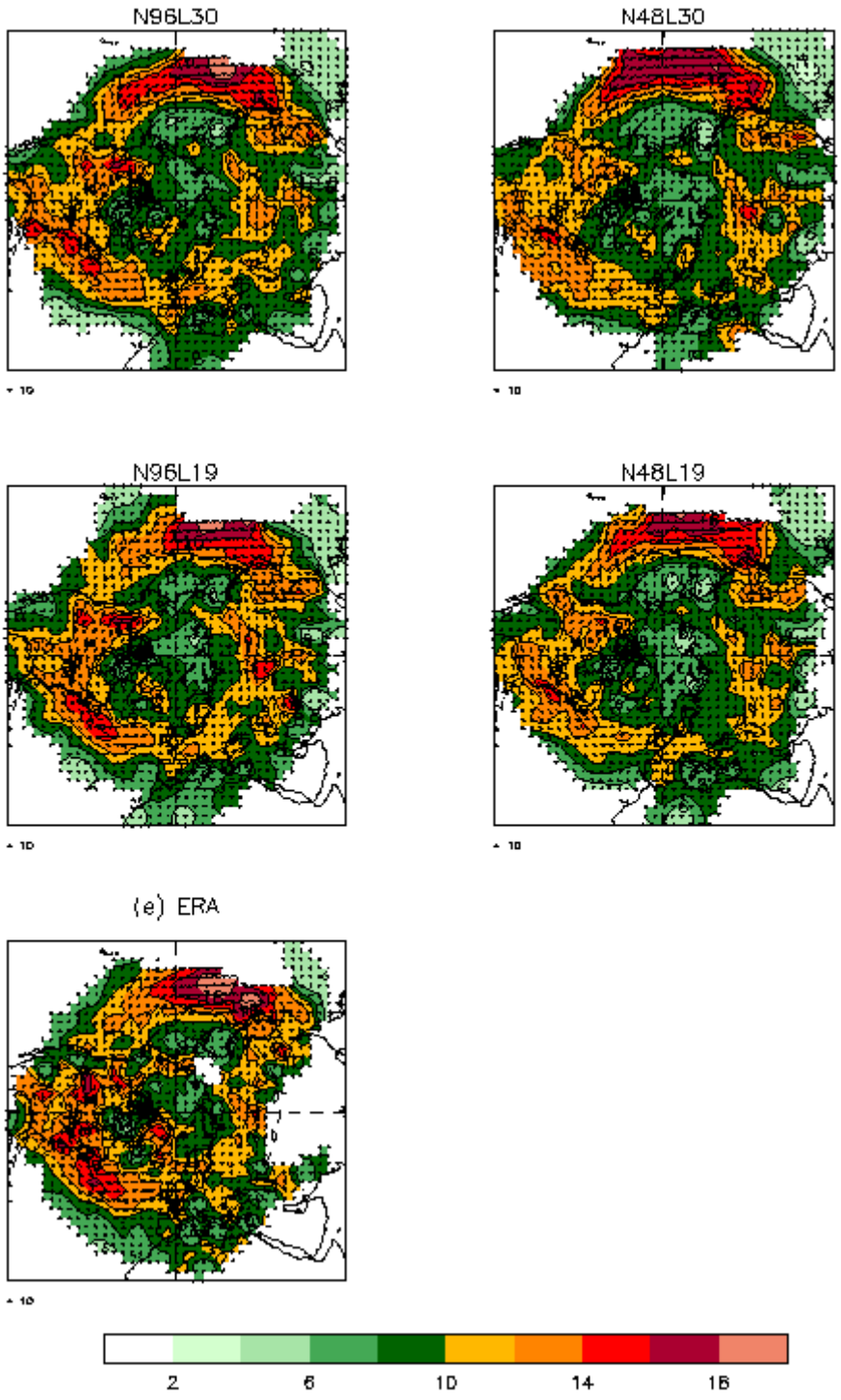

Figure 17

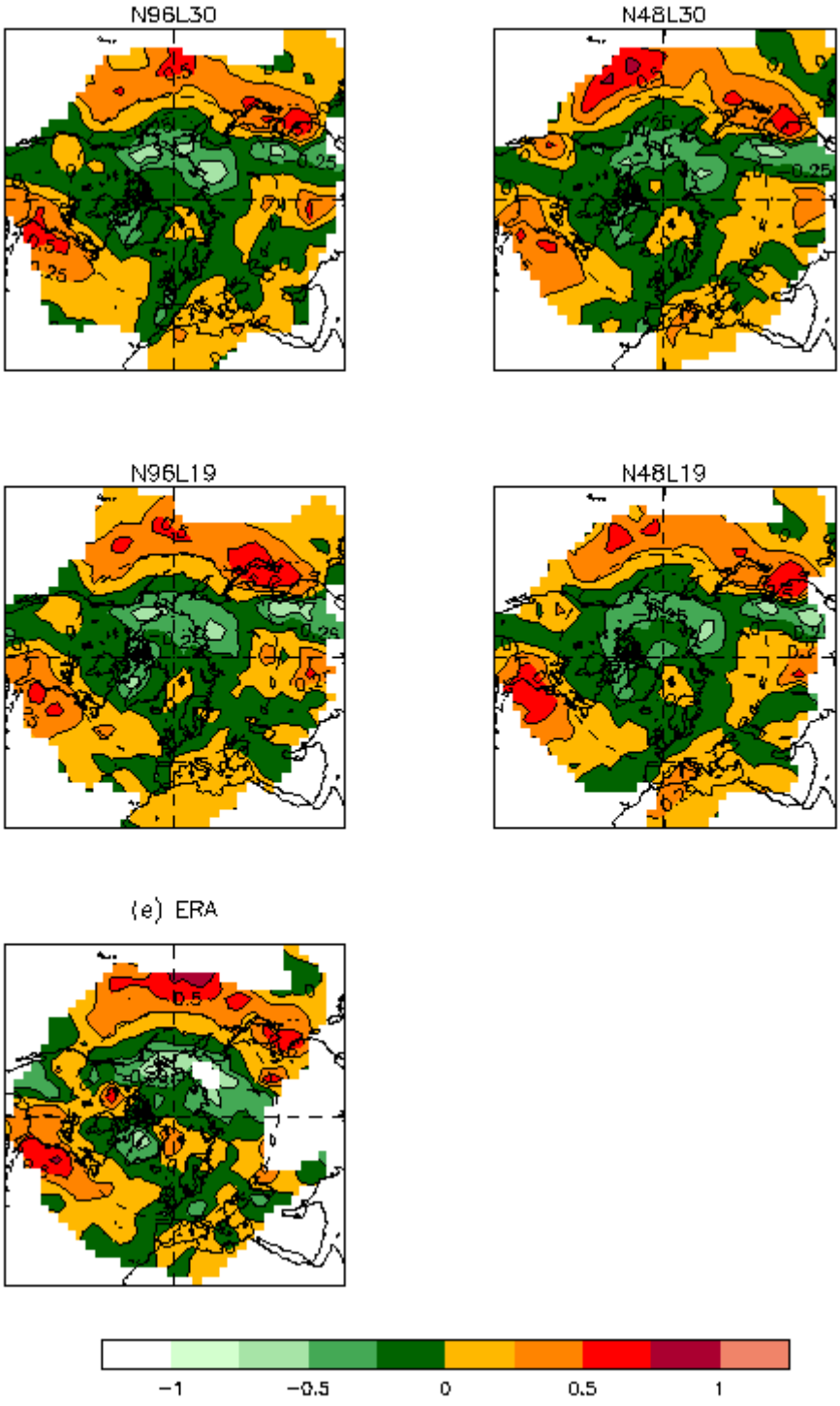

Figure 18

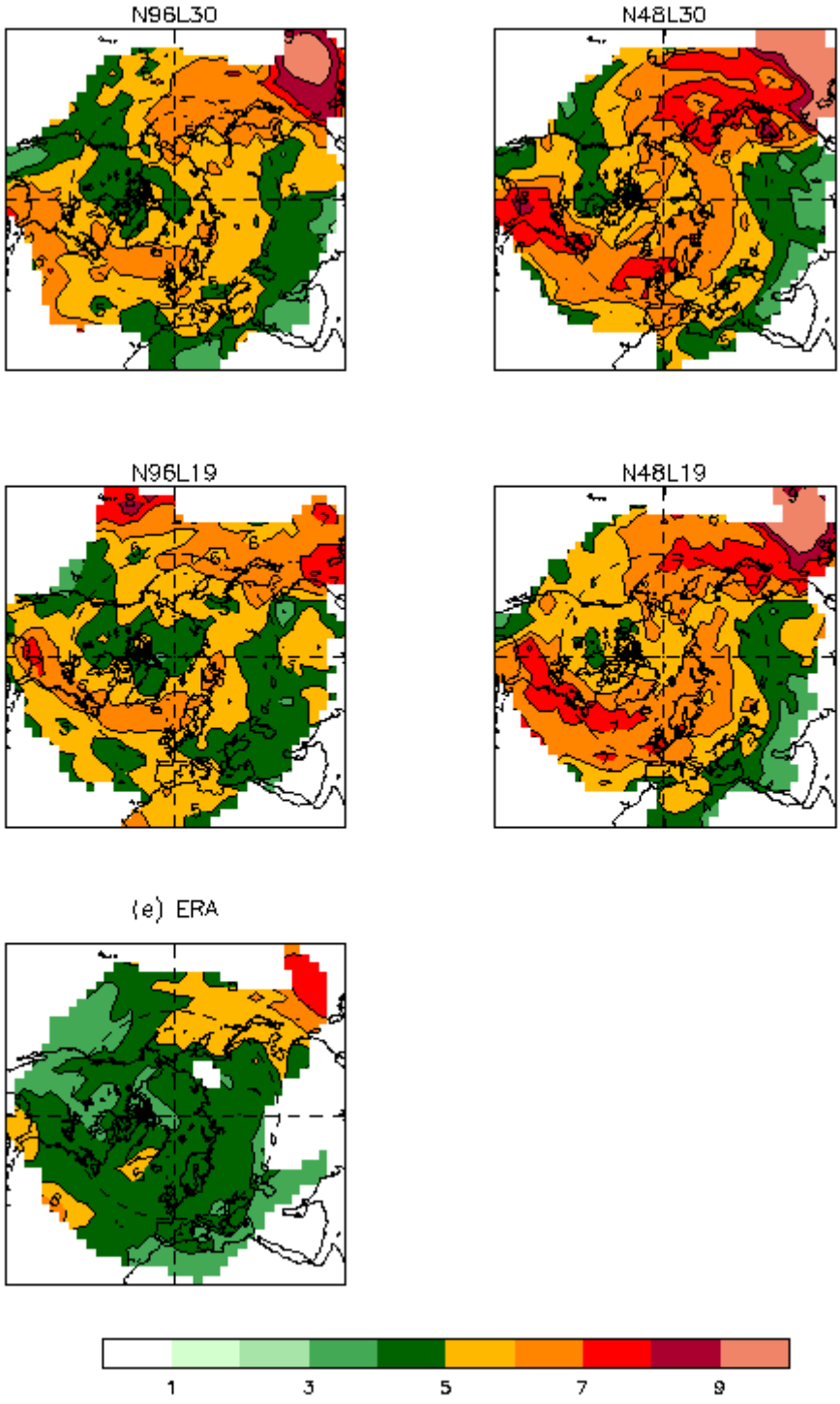

Figure 19

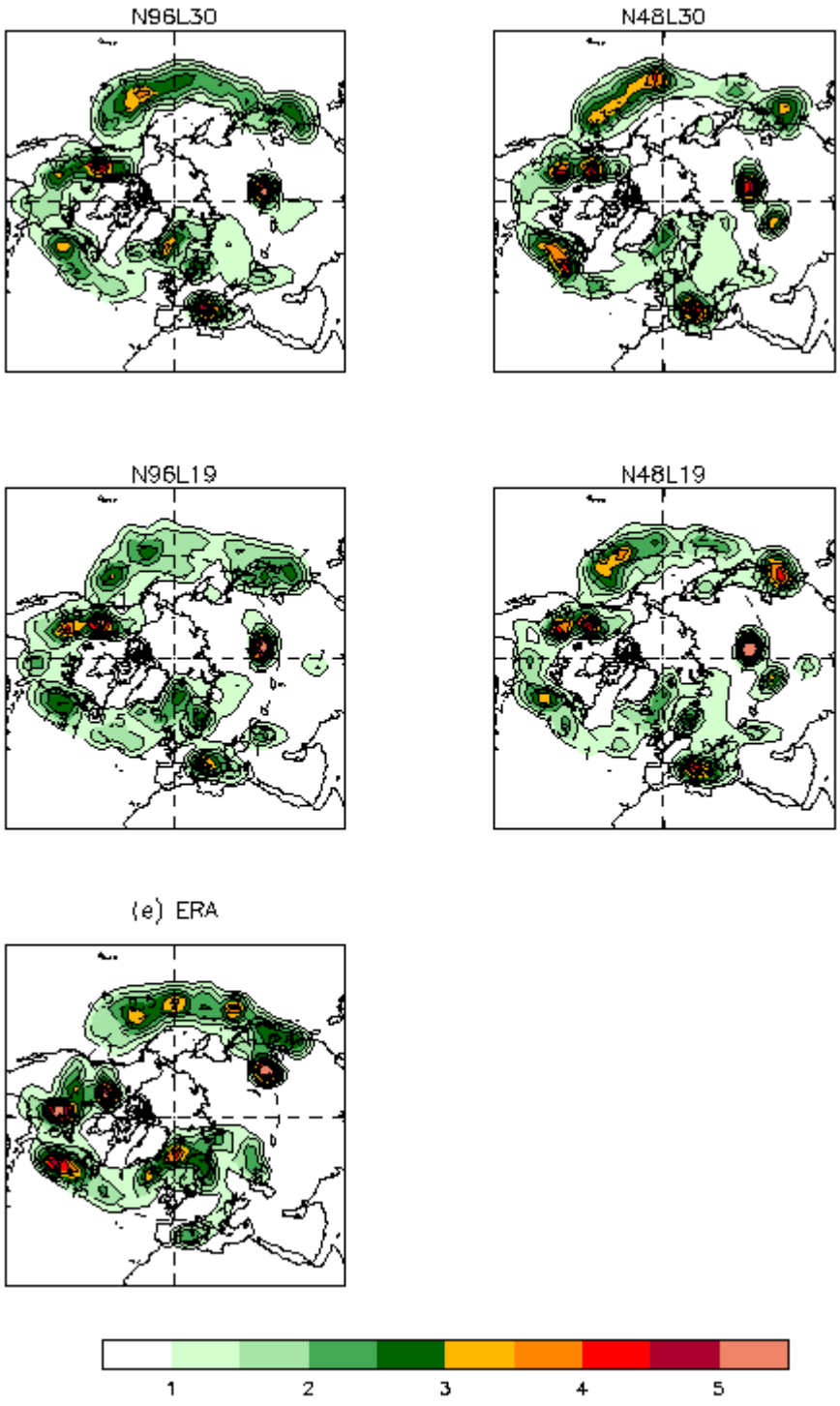

Figure 20

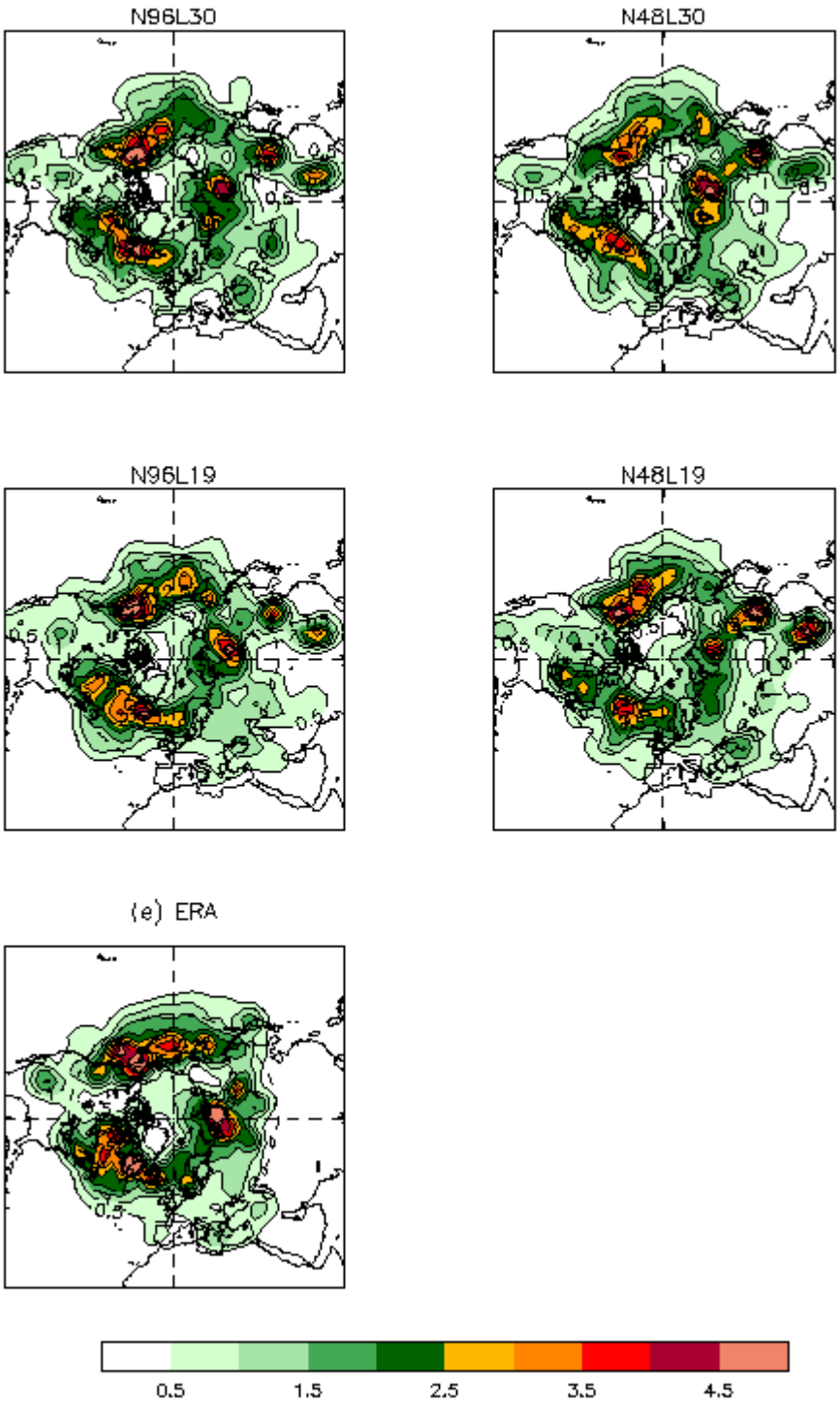

Figure 21